



Electron Density Variations in the Interstellar Medium and the Average Frequency Profile of a Scintle from Pulsar Scintillation Spectra

N. Bartel¹, M. S. Burgin² , E. N. Fadeev², M. V. Popov², N. Ronaghikhameneh^{1,3}, T. V. Smirnova⁴, and V. A. Soglasnov²

¹York University, 4700 Keele St., Toronto, ON M3J 1P3, Canada

²Lebedev Physical Institute, Astro Space Center, Profsoyuznaya 84/32, Moscow, 117997, Russia

³University of Alberta, 116 St. & 85 Ave., Edmonton, AB T6G 2R3, Canada

⁴Lebedev Physical Institute, Pushchino Radio Astronomy Observatory, Pushchino 142290, Moscow region, Russia

Received 2022 April 18; revised 2022 October 27; accepted 2022 October 28; published 2022 December 15

Abstract

We observed the scintillation pattern of nine bright pulsars at 324 MHz and three at 1.68 GHz and analyzed the wavenumber spectrum, which is related to electron density variations of the plasma turbulence of the interstellar medium (ISM). For all pulsars the frequency section of the autocorrelation function (ACF) of the dynamic spectra to at least 45% of the maximum corresponds to predictions of scattering theories with a range of power-law exponents of the wavenumber spectrum of $3.56 \leq \alpha \leq 3.97$ with errors ≤ 0.05 and a mean with standard deviation of 3.76 ± 0.13 . The range includes $\alpha = 3.67$ for the Kolmogorov spectrum. Similar results, although with larger errors, were found from the Fourier transform of the ACFs down to $\sim 10^{-3}$ of the maximum. No clear case of a distinction between thin-screen and extended-medium scattering models was found. The average frequency profile of the scintles can be characterized for steep wavenumber spectra with $\alpha \lesssim 4$ by a cusp with a somewhat rounded peak. For flatter spectra, down to at least $\alpha \sim 3.56$ the cusp with its peak becomes more pronounced and its decay steepens. We discuss our findings in the context of the scattering characteristics of the ISM.

Unified Astronomy Thesaurus concepts: [Interstellar scintillation \(855\)](#); [Radio pulsars \(1353\)](#); [Very long baseline interferometry \(1769\)](#); [Interstellar scattering \(854\)](#)

1. Introduction

Electron density variations in the interstellar medium (ISM) scatter radio emission from cosmic sources. The variations can be characterized by a spatial correlation function. Its Fourier transform (FT) is the spatial wavenumber spectrum with an exponent, α , that describes its steepness. Extensive studies of scattering effects began with the discovery of pulsars, since pulsars are quasi-point-like sources that provide a coherent flux of radio waves where the influence of the source structure can be neglected. Scattering leads to image blurring, pulse broadening, and intensity modulation over time and frequency. The observable parameters characterizing these phenomena are the scattering angle, θ_{sc} , the scattering time, τ_{sc} , the diffraction scintillation time, t_{scint} , and the decorrelation bandwidth, $\Delta f_{1/2}$. Theoretical considerations of scattering effects by, for example, Lovelace (1970), Lee & Jokipii (1975a, 1975b, 1975c), Rickett (1977), and Shishov et al. (2003) established early on a number of relationships between the characteristics of electron density variations and observable scattering parameters such as those given above.

Previously we reported on a comparison of θ_{sc} and τ_{sc} and our estimates of the distances to the effective scattering screens (Gwinn et al. 2016; Popov et al. 2017, 2020; Fadeev et al. 2018), as well as on the time characteristics of the scintillation pattern (Popov & Smirnova 2021).

In this paper we focus on the frequency characteristics of the scintillation pattern. The frequency section of the time-averaged autocorrelation functions, $ACF(\Delta f)$, of consecutive pulsar scintillation spectra, or dynamic spectra, is often used to

derive the parameter, $\Delta f_{1/2}$. This section, or its Fourier transform, $\mathcal{FT}[ACF(\Delta f)]$, can also be compared with predictions of thin-screen and extended-medium scattering models of plasma inhomogeneities in the intervening ISM, both for a Gaussian and a power-law spatial wavenumber spectrum with spectral index, α . While there have been many observational investigations of the parameter α , only very few, and then for only a few pulsars, were based on observing $ACF(\Delta f)$ functions and comparing them to model predictions (e.g., Armstrong & Rickett 1981; Wolszczan 1983).

New insights into the scattering process were obtained with the development of space very long baseline interferometry (VLBI) observations of pulsars with Radioastron, which allowed the predicted substructure (Goodman et al. 1987) of the visibility function to be discovered (Gwinn et al. 2016; Popov et al. 2017). On long ground-space baseline projections for which the scattering disk is fully resolved the visibility function retains values clearly larger than zero over a range of delays corresponding to the scattering time, τ_{sc} . Since τ_{sc} is inversely related to $\Delta f_{1/2}$, pulsars with a broad visibility function are expected to have a narrow decorrelation bandwidth, $\Delta f_{1/2}$. Therefore, depending on the time and frequency resolution of the observations, using the functions $ACF(\Delta f)$ and $\mathcal{FT}[ACF(\Delta f)]$ can be considered complementary for providing a more complete analysis of the dynamic spectra.

In this paper we report on an analysis of the dynamic spectra of 12 pulsars. The time range of the dynamic spectra is for each pulsar clearly longer than the scintillation time so that our results refer to an analysis of the scintillations in the averaging mode (Narayan 1992). We compare the dynamic spectra with the predictions of thin-screen and extended-medium scattering models in terms of the wavenumber spectral index, α , of the ISM electron density variations, discuss our results with measurements by others, search for hints for an observational preference for either of the models, relate the dynamic spectra

Table 1
List of Pulsars

PSR	P	DM	l_{II}	b_{II}	Obs.	N_f	N_t	Station	Date	f	Code
(1)	(s)	(pc cm ⁻³)	(deg)	(deg)	(minutes)	(7)	(8)	(9)	(yyyy mm dd)	(MHz)	(12)
B0329+54	0.714	26.7	145.0	-1.2	60	4096	504	GB	2012 11 26	324	raes10a
B0525+21	3.745	50.9	183.4	-6.9	168	512	2700	AR	2013 09 18	1676	raks02ac
B0823+26	0.531	19.4	197.0	31.7	150	2048	16900	AR	2015 03 11	324	rags04aj
B0834+06	1.274	12.8	219.7	26.3	55	8192	3300	GB	2014 12 08	324	rags04ah
B0919+06	0.430	27.3	225.4	36.4	90	2048	5200	AR	2018 05 10	324	rags29p
B1133+16	1.188	4.8	241.9	69.2	120	1024	6000	AR	2018 02 03	324	rags29g
B1237+25	1.382	9.3	252.0	86.5	100	512	4340	AR	2017 12 22	324	rags29c
B1642-03	0.387	35.7	14.1	26.1	90	512	13200	WB	2013 08 09	324	raks02ab
B1749-28	0.562	50.8	1.5	-1.0	250	192	2450	PA	2014 05 26	1676	raks02az
B1929+10	0.226	3.2	47.4	-3.9	100	512	26000	AR	2015 05 05	324	rags04ao
B1933+16	0.359	158.5	52.4	-2.1	90	8192	15036	AR	2013 08 01	1676	rags02aa
B2016+28	0.558	14.1	68.0	-4.0	45	2048	5300	AR	2015 05 22	324	rags04aq

Note. Columns are as follows: (1) pulsar name; (2) pulsar period; (3) dispersion measure; (4) galactic longitude; (5) galactic latitude; (6) observing time range for dynamic spectra; (7) number of frequency channels across the bandpass; (8) number of spectra over the observing time range; (9) radio telescope station: AR—Arecibo, GB—Green Bank (GBT), PA—Parkes, WB—Westerbork; (10) observing date; (11) center of observing frequency; (12) code of observing session.

to the characteristics of the substructure in the visibility functions, and infer the average frequency profile of the scintles as a function of α .

2. Observational Parameters of the Dynamic Spectra

We studied the pulsar dynamic spectra for nine pulsars at a center frequency of 324 MHz and for three pulsars at 1676 MHz. The data were obtained with VLBI recorders over a bandwidth of 16 MHz in the context of the space VLBI Radioastron scientific program (Kardashev et al. 2017). We list the pulsars together with their periods, dispersion measures, galactic coordinates, recording stations, dates of observations, and observing frequencies in Table 1. The data were already used earlier in our other studies (refer to “Code” in Table 1), and more details on these observations and the first stage of data analysis are given in our previous papers (see above).

Each dynamic spectrum, $S(f_i, t_j)$ as a function of frequency, f , and time, t , consists of $N_f \times N_t$ values, with $1 \leq i \leq N_f$ and $1 \leq j \leq N_t$, where N_f is the number of frequency channels covering the frequency range in the bandpass from 316 to 332 MHz or from 1668 to 1684 MHz, and N_t is the number of individual spectra in a given set of observations. We calibrated the dynamic spectra as follows:

$$S(f_i, t_j) = \frac{S^{\text{on}}(f_i, t_j) - S^{\text{off}}(f_i, t_j)}{S^{\text{off}}(f_i, t_j)}, \quad (1)$$

and hereafter refer to them simply as $S(f, t)$. Here, S^{on} and S^{off} are the spectra obtained during the on-pulse and off-pulse windows. Usually, the time interval between successive spectra is equal to the period of the pulsar, but in some cases averaging was done over several periods to smooth out the intensity fluctuations from pulse to pulse. The time span for the dynamic spectra, as well as N_f and N_t , is also listed in Table 1.

In Figure 1 we give examples of dynamic spectra for four pulsars: B0525+21, B0919+06, B1133+16, and B1642-03. The dynamic spectra for the other eight pulsars in our sample were already published earlier (Popov et al. 2016, 2021; Fadeev et al. 2018). One can see islands of increased intensity distributed randomly over the time–frequency domain. These are the peaks of diffractive structure, which we refer to as

“scintles.” In particular, we are interested in the decorrelation bandwidth, $\Delta f_{1/2}$, the frequency section of the autocorrelation function, $\text{ACF}(\Delta f)$, as well as the Fourier transform of this function, their relation to parameters of the turbulent interstellar plasma, and the average frequency profile of the scintles.

3. Analysis of the Dynamic Spectra

3.1. Frequency Structure of the Dynamic Spectra and their Relation to the Turbulent Plasma of the Intervening ISM

Scintillations of pulsars are related to electron density fluctuations in the ISM, which can be characterized by a spatial correlation function. Its Fourier transform is the spatial wavenumber spectrum, $P(q)$. If the magnitude of the three-dimensional wavenumber, q , is within a limited range of wavenumbers with inner and outer boundaries, then $P(q)$ can be described as a power law, $P_P(q) = C_n q^{-\alpha}$, with $\alpha < 4$ (Romani et al. 1986) including $\alpha = 11/3$ for a Kolmogorov spectrum. For a Gaussian the spectrum is $P_G(q) = G_n \exp(-(q/q_0)^{-2})$, corresponding to $\alpha = 4$. The value of α can be obtained from the two-dimensional ACF of $S(f, t)$ at zero time lag, $\text{ACF}(\Delta f, \Delta t = 0)$. For simplicity, we refer to this frequency section after normalization as $\text{ACF}(\Delta f)$ with

$$\text{ACF}(\Delta f) = \langle S(f, t)S(f + \Delta f, t) \rangle_t. \quad (2)$$

The frequency section, $\text{ACF}(\Delta f)$, is predicted to depend on α . For a thin-screen model of the ISM analytical solutions exist for the Gaussian and power-law models that can be fit to the ACFs. For an extended-medium model of the ISM (e.g., Lee & Jokipii 1975a) analytical solutions for the frequency section of the ACF exist for the Gaussian spectrum but only numerical solutions for the power-law spectrum (Lee & Jokipii 1975b).

Instead of computing the frequency section, $\text{ACF}(\Delta f)$, for comparison with predictions, some authors have preferred to compare the Fourier transform of this ACF with predictions. Both approaches can be considered complementary. In this paper we use both approaches, by following Wolszczan (1983) concerning the computation of the predictions of the extended-medium scattering model and Armstrong & Rickett (1981) concerning the thin-screen model.

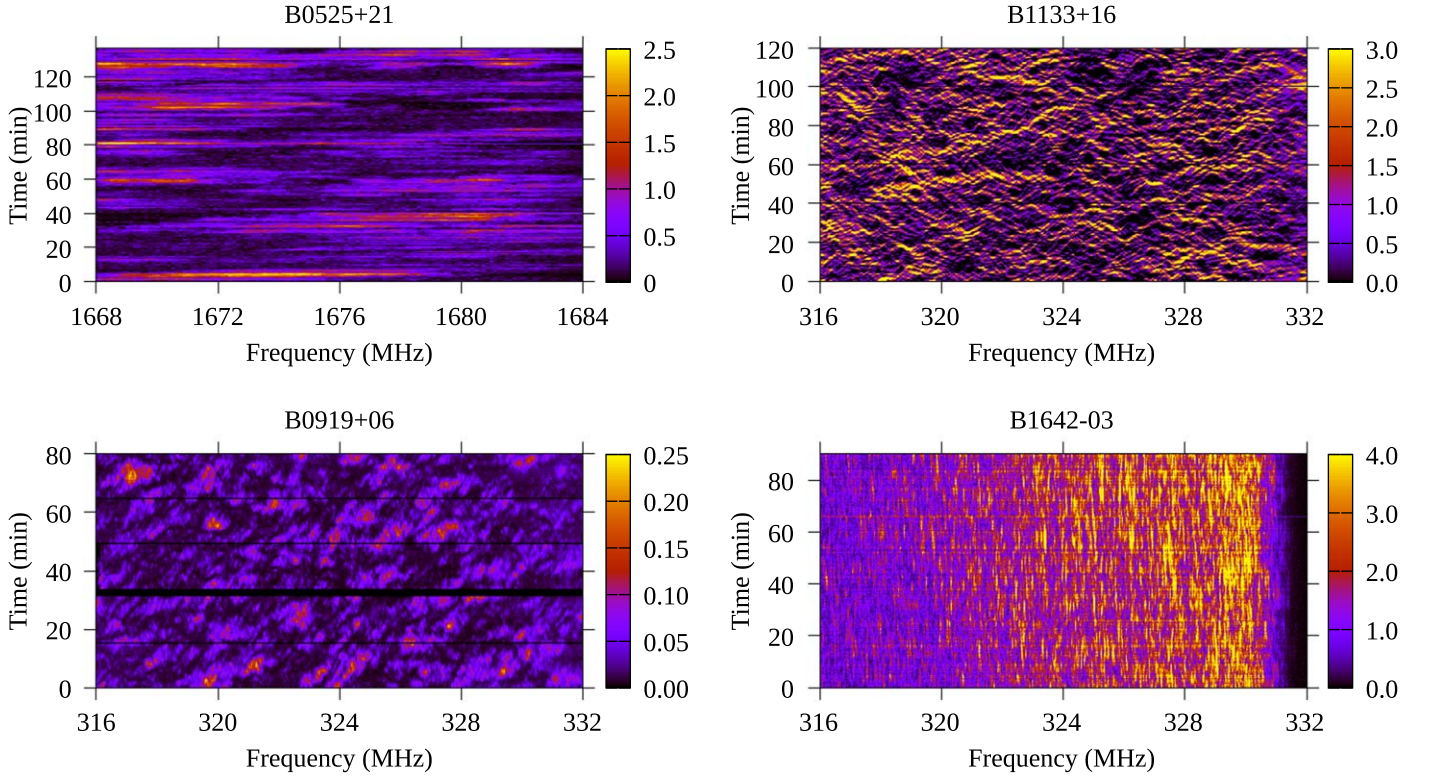


Figure 1. Dynamic spectra of four pulsars analyzed in this paper. The color-coded intensity as a function of time and frequency is given in arbitrary units in the bar on the right side of each spectrum.

Table 2
Results of Data Reduction

PSR	$\Delta f_{1/2}$ (kHz)	$\Delta \tau_{1/2}$ (μ s)	σ_{stat} (10^{-2})	α_{ACF}	rms_{ACF} (10^{-2})	$\alpha_{\mathcal{FT}(\text{ACF})}$	$\text{rms}_{\text{scat. type}}$ (10^{-2})	Scat. Type
(1)	(2)	(3)	(4)	(5)	(6)	(7)	(8)	(9)
B0329+54	30	7.90	1.0	3.67 ± 0.02	0.05	3.80 ± 0.05	0.15	K
B0525+21	4000	0.04	8.6	3.73 ± 0.02	0.5	3.80 ± 0.05	3.1/4.2/4.2	K/E/L
B0823+26	180	0.83	1.2	3.56 ± 0.02	0.2	3.60 ± 0.05	1.8	K
B0834+06	400	0.55	5.8	3.74 ± 0.02	0.2	4.00 ± 0.10	1.8	K
B0919+06	170	1.15	1.9	3.59 ± 0.02	0.2	3.70 ± 0.10	1.7	K
B1133+16	96	2.50	0.7	3.80 ± 0.02	0.3	4.00 ± 0.10	2.3/3.7	K/L
B1237+25	2300	0.11	3.3	3.90 ± 0.04	0.7	3.80 ± 0.10	2.7/3.8	G/E
B1642-03	930	0.20	4.0	3.97 ± 0.05	1.4	3.80 ± 0.20	3.0/3.7	G/E
B1749-28	690	0.31	3.5	3.78 ± 0.02	0.2	3.90 ± 0.10	3.7/3.8/3.9	E/L/K
B1929+10	970	0.39	6.8	3.85 ± 0.02	0.4	3.90 ± 0.10	2.8	E
B1933+16	120	6.85	1.1	3.64 ± 0.04	0.7	3.80 ± 0.10	1.7	K
B2016+28	71	2.04	4.9	3.92 ± 0.02	0.2	3.90 ± 0.05	1.1/1.7	L/E

Note. Columns are as follows: (1) pulsar name; (2) HWHM of the ACFs of the dynamic spectra at zero time lag (the smaller value for for B1643-03 of ~ 6 kHz is not considered in this paper); (3) HWHM of the $\mathcal{FT}(\text{ACF})$ s; (4) fractional rms uncertainty of values in columns (2) and (3); (5) parameter α , from the fit of the extended-medium scattering model to the observed ACFs down to 0.45 of the maximum; the errors were calculated from the statistical errors derived from column (6) added in quadrature with systematic errors estimated from slight deviations of the ACF from the model (same values for extended-medium and thin-screen models); (6) the rms values in units of correlation coefficients for the ACFs with respect to the fit model; (7) parameter α , from the fit of the extended-medium scattering model to the Fourier transforms of the observed ACFs for the delay range from 0.2 to $20 \Delta \tau / \Delta \tau_{1/2}$ or down to $\sim 10^{-3}$ of the maximum (same values for extended-medium and thin-screen models); the errors are largely systematic errors estimated from non-random deviations of $\mathcal{FT}(\text{ACF})$ from the models; (5), (7) values including errors larger than 4 are still valid but nonphysical within the context of the models and may indicate deviations from them; (8) the smallest rms values in units of (10^{-2}) of the maximum of unity of the observed ACFs with respect to the analytical $\text{ACF}(f)$ functions in column (9) from Table 4 up to $2 \times \Delta f / \Delta f_{1/2}$ (see Figure 7); (9) the best-matching functions from the four functions from Table 4, $\text{ACF}(G)$ to $\text{ACF}(K)$.

3.2. Determination of the Power-law Spectral Index, α , of the Wavenumber Spectrum

We studied 12 pulsars by analyzing the frequency section, $\text{ACF}(\Delta f)$, of the dynamic spectra. From $\text{ACF}(\Delta f)$ we

determined the decorrelation bandwidth, $\Delta f_{1/2}$, as the half-width at half maximum (HWHM), and list the values for each pulsar in Table 2. The fractional statistical (rms) error can be estimated as the inverse square root of the number of scintles in

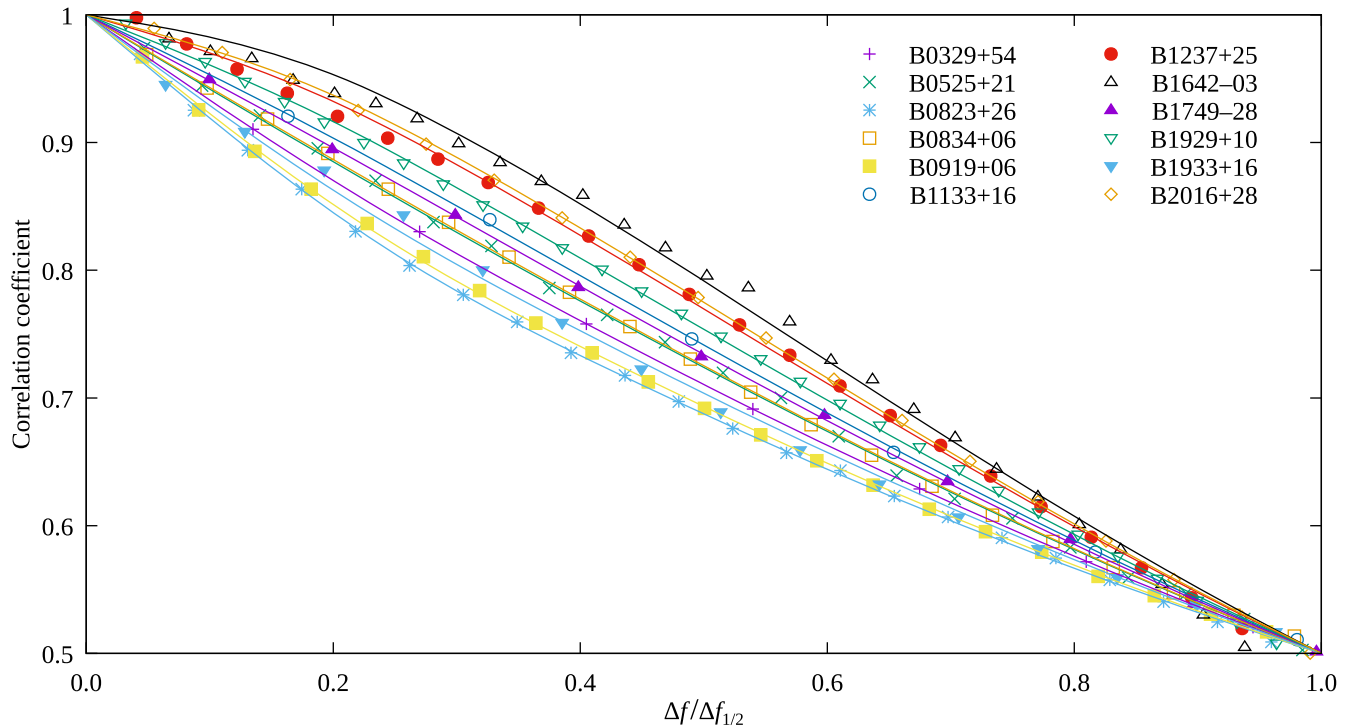


Figure 2. Comparison of the predictions from the extended-medium model of Lee & Jokipii (1975b) with computed autocorrelation functions for our 12 pulsars. The predictions are plotted as solid lines for indices of α corresponding to the best-fitting models. The ACFs are plotted as data points with different symbols for each of the pulsars listed on the upper right.

each dynamic spectrum (Backer 1975). An approximate expression is given by $\sigma_{\text{stat}} = \left(f_s \frac{BT_{\text{obs}}}{\Delta f_{1/2} t_{\text{scint}}} \right)^{-1/2}$, where f_s is the filling factor, B the receiver bandwidth, T_{obs} the observing time, and t_{scint} the scintillation time. Assuming $f_s = 0.5$, and taking values for t_{scint} from Popov & Smirnova (2021), we list σ_{stat} in Table 2. For a consideration of possible systematic errors, see Popov & Smirnova (2021).

We fit the functions with a curve corresponding to the predictions for the extended-medium model. The differences between the predictions for $\text{ACF}(\Delta f)$ for the thin-screen and the extended-medium models are small for the inner part but larger for the tail of the functions. Using, for instance, the solutions for the Gaussian spectrum ($\alpha = 4.0$; Lovelace 1970; Chashei & Shishov 1976; Lerche 1979) with a maximum at unity and scaling them so that the values for $\Delta f_{1/2}$ are identical, the functions differ by less than 0.002 down to the HWHM and by less than 0.007 down to 20% of the maximum. These differences are not large enough to be considered for our analysis of the inner part of $\text{ACF}(\Delta f/\Delta f_{1/2})$ but have to be considered for the tail of the ACFs, where they could perhaps become measurable. Although for some pulsars a good fit could be obtained even for the tail of $\text{ACF}(\Delta f/\Delta f_{1/2})$, a consistently good fit for all pulsars was only obtained up to frequency lags, $\Delta f/\Delta f_{1/2} \sim 1.2$, where $\text{ACF}(\Delta f/\Delta f_{1/2}) = 0.45$. For this range, the fitted values of α for the two scattering models were the same within our sensitivity limits. We list the values of α together with their uncertainties in Table 2.

For a summary view of our 12 measured $\text{ACF}(\Delta f/\Delta f_{1/2})$ functions we plot their inner portions down to half of the maximum and compare them with the fit model predictions in Figure 2. It can be seen that the value of α is mostly determined by the shape of the inner part of $\text{ACF}(\Delta f/\Delta f_{1/2})$. All the

functions are within a range of fit parameters, α , between 3.56 for the lower curve of PSR B0823+26 and 3.97 for the upper curve of PSR B1642-03. The mean with standard deviation is $\langle \alpha_{\text{ACF}} \rangle = 3.76 \pm 0.13$ and is therefore close to $\alpha_K = 3.67$ of the Kolmogorov spectrum. The quality of the fit varies. We list rms variations of the observed ACFs from the model for each pulsar in Table 2. The fits are for most pulsars quite good, with rms values smaller or equal to 0.005 on the scale of the ACF functions down to 0.45 of the maximum of unity. Larger deviations with rms values of 0.007–0.014 were found for PSRs B1237+25, B1642-03, and B1933+16. These are mostly not random variations but to a large part systematic deviations from the model.

To inspect the fits in more detail down to lower correlation coefficients, we plot $\text{ACF}(\Delta f/\Delta f_{1/2})$ with the models from Figure 2 for each of the 12 pulsars separately for frequency lags up to $2 \times \Delta f_{1/2}$ in Figure 3. For about half the pulsars the data are still well fit by the model over the wider range of frequency lags. However, significant deviations are now apparent for the other half.

Some of these deviations in the tail of $\text{ACF}(\Delta f/\Delta f_{1/2})$ could be due to technical effects such as (1) superposition of the contribution from neighboring scintles; (2) the limited band of the receiver filter, which distorts or cuts off wide diffraction structures; (3) inaccuracy of the determination of the off-pulse level for the computation of ACFs; and (4) relatively low signal-to-noise ratios. Some of these effects, if not all, could possibly increase the ACFs toward large lags. Such increase can be seen for PSRs B0834+06 and B1133+16. For the other pulsars with deviations, the tail of the ACFs is lower than the model predictions. In these cases the deviations are likely indications of deficiencies in the scattering models.

A complementary method to estimate α values is to fit the models to the Fourier transform of the ACFs, $\mathcal{FT}(\text{ACF})$ (e.g.,

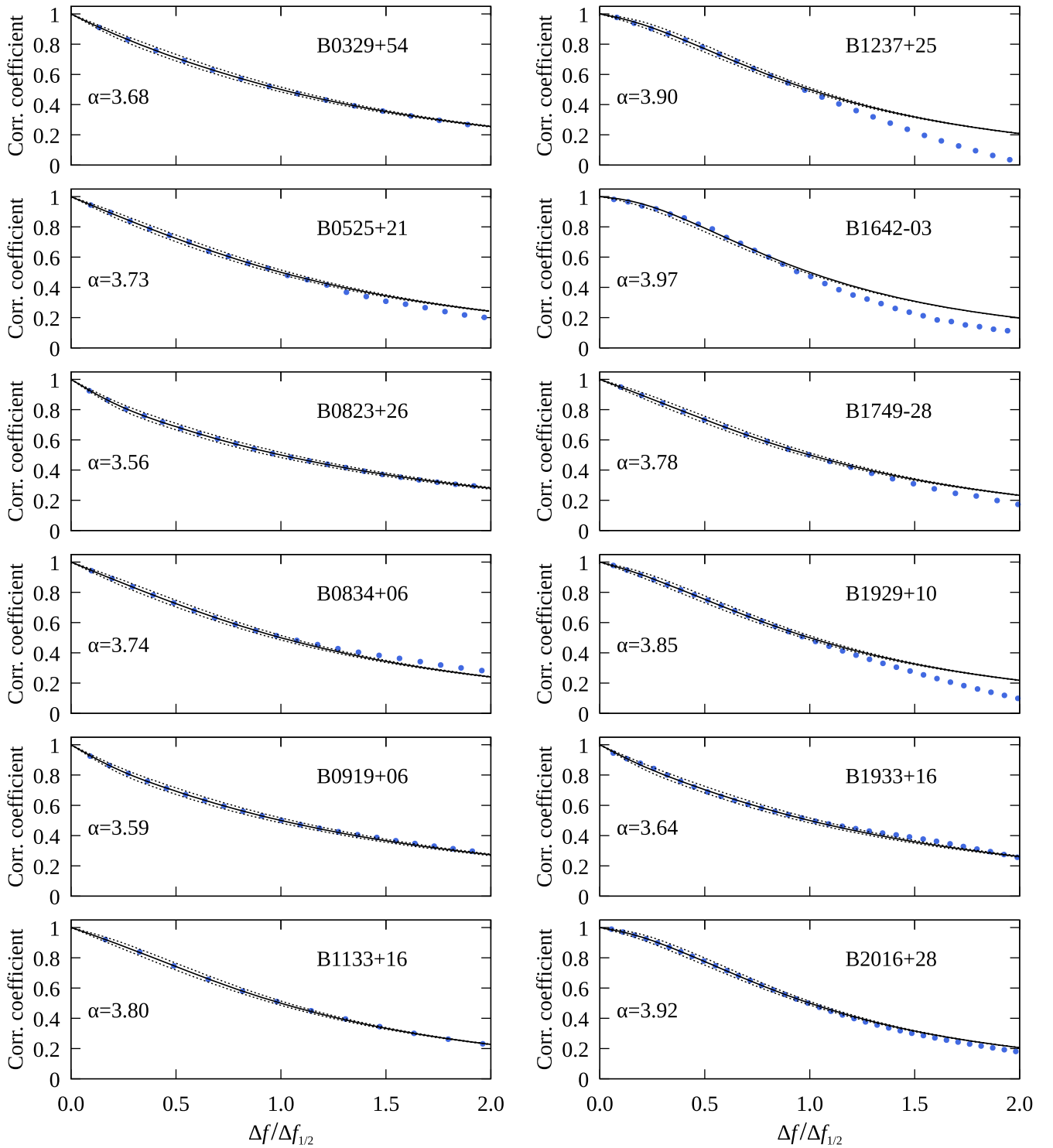


Figure 3. Comparison of the $\text{ACF}(\Delta f)$ functions derived from the observations (blue dots) with the theoretical predictions for the extended-medium scattering theories with power-law spectral index, α , as a fitting parameter. The solid line shows the best-fitting model for the inner part of the $\text{ACF}(\Delta f)$ down to 45% consistently for all pulsars. The surrounding dotted lines indicate $\Delta\alpha = \pm 0.05$ deviations from the best-fit value for illustration purposes. For better comparison all functions were normalized by their HWHM frequency lags, $\Delta f_{1/2}$.

Armstrong & Rickett 1981; Wolszczan 1983). We computed $\mathcal{FT}[\text{ACF}(\Delta f)]$ by using the full range of frequency delays of ± 4 MHz. To suppress fluctuations, we applied to the observed $\text{ACF}(\Delta f)$ functions a Gaussian filter with a half-width at the $1/e$ level of $4 \times \Delta f_{1/2}$. Only for PSR B0525+21, with its relatively large value of $\Delta f_{1/2}$, did we use a four times narrower Gaussian.

A comparison of the observed functions $\mathcal{FT}[\text{ACF}(\Delta f)]$ of all pulsars with the theoretical predictions for the extended-medium and for the thin-screen models is shown in Figure 4. In this subsection we focus on the fit of the former to the $\mathcal{FT}(\text{ACF})$ s. All $\mathcal{FT}(\text{ACF})$ functions are normalized in amplitude and in width. Their HWHM values, $\Delta\tau_{1/2}$, are listed in Table 2.

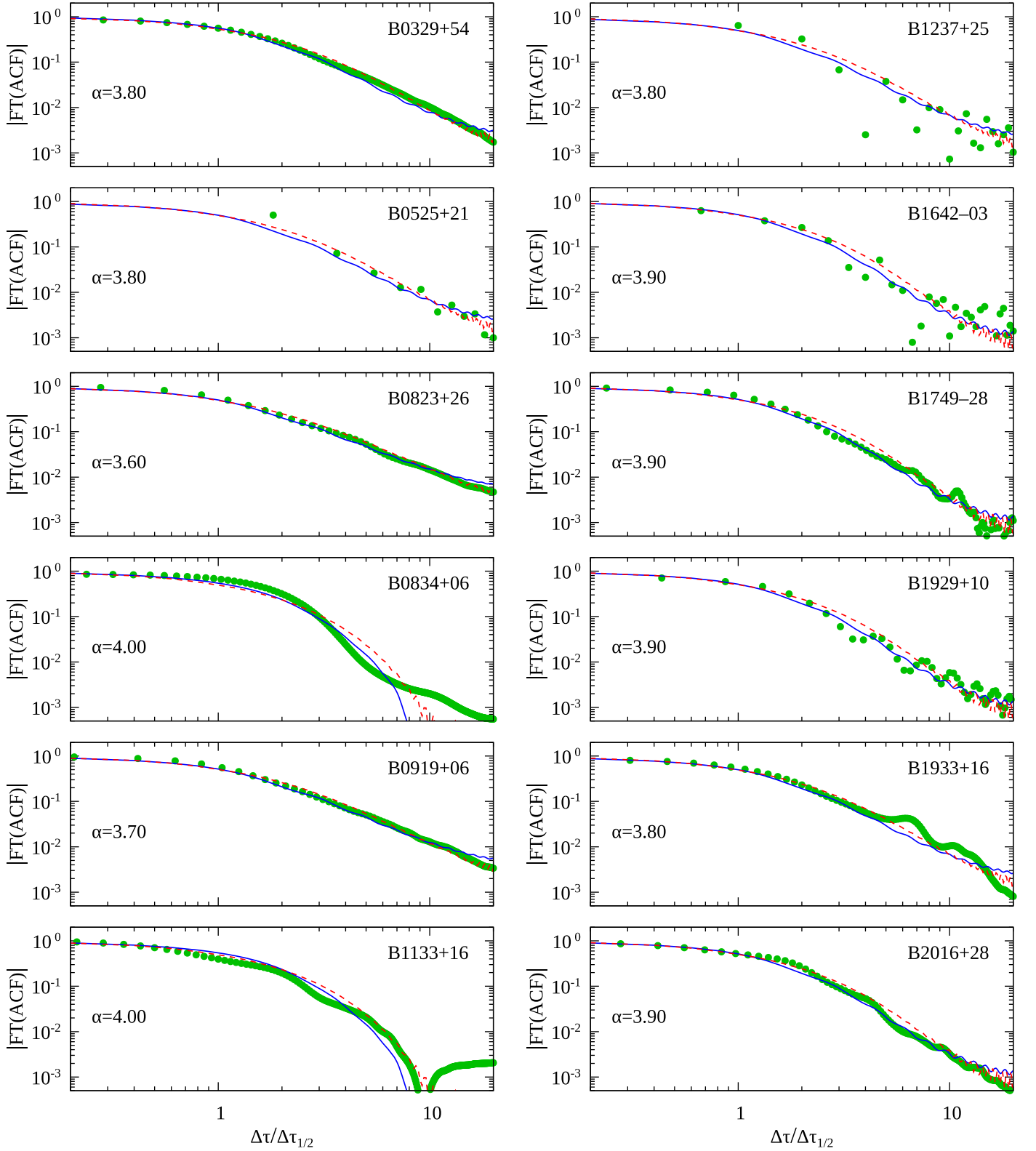


Figure 4. The magnitude of the Fourier transform of the observed ACFs, $|\mathcal{FT}(\text{ACF})|$ (green dots), fit by the theoretical predictions for the extended-medium scattering theory with rounded power-law spectral index α (solid blue lines) and for the thin-screen model (dashed red lines) with the same value for α . Scattered points in the tail of some functions are due to noise. Delay is given as $\Delta\tau$ with $\Delta\tau_{1/2}$ as the HWHM listed in Table 2.

The values of $\alpha_{\mathcal{FT}(\text{ACF})}$ and their estimated errors are listed in Table 2 (column (7)). The mean with standard deviation is $\langle\alpha_{\mathcal{FT}(\text{ACF})}\rangle = 3.83 \pm 0.12$, larger by 0.07 than $\langle\alpha_{\text{ACF}}\rangle$. The mean of the magnitudes of the differences to those obtained

from the fits to the ACFs with standard deviation is $\langle|\alpha_{\text{ACF}} - \alpha_{\mathcal{FT}(\text{ACF})}|\rangle = 0.11 \pm 0.07$. In general the values are fairly consistent within the errors given that the fitting ranges are quite different. The largest discrepancy is 0.26 for PSR

Table 3
Comparison of Estimates of α

PSR (1)	$\alpha_{\text{ACF}(\Delta f)}$ (2)	$\alpha_{\mathcal{FT}(\text{ACF})}$ (3)	$\alpha_{\mathcal{FT}(\text{ACF})}$ (4)	$\alpha_{\mathcal{FT}(\text{ACF})}$ (5)	α_{SF} (6)	$\alpha_{\Delta f_{1/2}(f)}$ (7)
B0329+54	3.68 ± 0.02	3.80 ± 0.05	3.85	3.7-4.0	3.67 ± 0.01	$3.41^{+0.41}_{-0.25}$
B0525+21	3.73 ± 0.02	3.80 ± 0.05				
B0823+26	3.56 ± 0.02	3.60 ± 0.05			3.66 ± 0.01	
B0834+06	3.74 ± 0.02	4.00 ± 0.10			3.528 ± 0.006	
B0919+06	3.59 ± 0.02	3.70 ± 0.10			3.57 ± 0.01	
B1133+16	3.80 ± 0.02	4.00 ± 0.10	3.90	3.4-3.8	3.86 ± 0.01	
B1237+25	3.90 ± 0.04	3.80 ± 0.10			3.39 ± 0.01	
B1642-03	3.97 ± 0.05	3.80 ± 0.20		3.2-3.9		$3.63^{+0.29}_{-0.21}$
B1749-28	3.78 ± 0.02	3.90 ± 0.10			3.82 ± 0.01	$3.50^{+0.18}_{-0.14}$
B1929+10	3.85 ± 0.02	3.90 ± 0.10			3.65 ± 0.02	
B1933+16	3.64 ± 0.04	3.80 ± 0.10	3.90		3.18 ± 0.01	$3.80^{+0.14}_{-0.12}$
B2016+28	3.92 ± 0.02	3.90 ± 0.05			$3.36 \pm 0.02^*$	

Note. Columns are as follows: (1) pulsar name; (2) taken from Table 2, column (5); (3) taken from Table 2, column (7); (4) estimates of α of the extended-medium power-law model from the Fourier transform of the frequency ACFs, PSRs B0329+54 (327 and 480 MHz), B1133+16 (327 MHz), and B1933 (1416 MHz; Wolszczan 1983); (5) estimate of α of the thin-screen power-law model from the Fourier transform of the frequency ACFs, PSRs B0329+54 (340, 408 MHz), B1133+16 (340 MHz), and B1642-03 (340 MHz; Armstrong & Rickett 1981); (6) estimate of α of the power-law spectrum from the structure function of the time section of the ACFs, with “*” indicating a measurement biased toward lower values (Popov & Smirnova 2021); (7) estimate of α of the power-law model from the decorrelation bandwidth, $\Delta f_{1/2}$, as a function of observing frequency in the range 80–8100 MHz, (Cordes et al. 1985).

B0834+06. The difference could perhaps at least partly be due to the large deviations from the model in the ACF for lags outside the ACF fitting range.

3.3. Comparison with Other Estimates of α

The exponent, α , of the wavenumber power-law spectrum of electron density variations can be estimated by several methods. In Table 3 we compare our estimates from Table 2 in columns (5) and (7) with those from other authors derived from the Fourier transform of the frequency section of the ACFs, structure function, and frequency dependence of the decorrelation bandwidth.

The most similar analysis to ours was done by Wolszczan (1983, column (4)) and Armstrong & Rickett (1981, column (5)) with data taken some 30 years before ours, who fit an extended-medium and a thin-screen scattering model, respectively, to the FTs of the ACFs. Compared with the values of Wolszczan (1983), our corresponding values in column (3) are all consistent with theirs within our errors. Compared with the values of Armstrong & Rickett (1981), which are given with relatively large ranges, ours are within their ranges or slightly above but exclude the range below $\alpha = 3.5$.

The values in the other columns were obtained with different analyses schemes. The most interesting for a comparison are those listed in column (6), which are based on the same data as ours in columns (2) and (3). They are derived from the structure function of the time section of the ACFs and are therefore best compared with our values in column (2). For five pulsars, the differences in α are ≤ 0.10 . For the other four pulsars, ignoring B2016+28 (see caption of Table 3), the differences are as large as 0.51 as for B1237+25.

The last column lists estimates of α obtained from a fit of the decorrelation bandwidth as a function of observing frequency. They are consistent with our values in column (2) within 1.5 times their larger uncertainties. We comment on these comparisons in Section 4.

3.4. Thin Screen or Extended Medium?

To search for any indications whether a thin-screen or an extended-medium scattering model is preferred by our observed $\text{ACF}(\Delta f)$ functions, we extend the functions to frequency lags of $4.5 \times \Delta f_{1/2}$ and plot the observed ACFs from Figure 3 together with the predictions of the two scattering models in Figure 5. For pulsars with broad scintles relative to the bandwidth of 16 MHz (see, e.g., PSR B0525+21; Figure 1 and Table 2), we plot the functions only for a portion of the total range in frequency lags.

Slight differences in the models can be seen at $\Delta f \sim 2.5 \times \Delta f_{1/2}$ that grow larger with further frequency lags. For most pulsars the tail of the measured ACFs deviates substantially from either of the models and, as discussed in Section 3.2, can likely be interpreted in most cases as being due to deficiencies in the theoretical scattering models.

Three pulsars, B0329+54, B0823+26, and B0919+06, show fairly good consistency in the observed ACFs with either or both of the models for frequency lags at least up to $4.5 \times \Delta f_{1/2}$. For PSRs B0329+54 and B0919+06, deviations from either of the two models clearly grow for even larger lags. PSR B0823+26, however, is a candidate that warrants more scrutiny. In Figure 6 we show the observed ACF and the two model curves but now up to $\Delta f \sim 6 \times \Delta f_{1/2}$. The extended-medium model is drawn as in Figure 5 with $\alpha_{\text{em}} = 3.56$. The thin-screen model curve lies for the same α value above the extended-medium model curve and is therefore a candidate for matching the tail of the ACF, but not that much that it would be a good fit to the observed ACF. To investigate this case further, we plot the thin-screen model for $\alpha_{\text{ts}} = 3.49$, 3.5σ below the best-fit value in an attempt to deviate not too much from the best fit but also to match the tail of the ACF. However, even in this extreme case, deviations much larger than for the inner part of the ACF are still visible. We therefore think that also in this case the deviations are due to effects discussed already for the other pulsars. There is no convincing case that either of the two models is preferred.

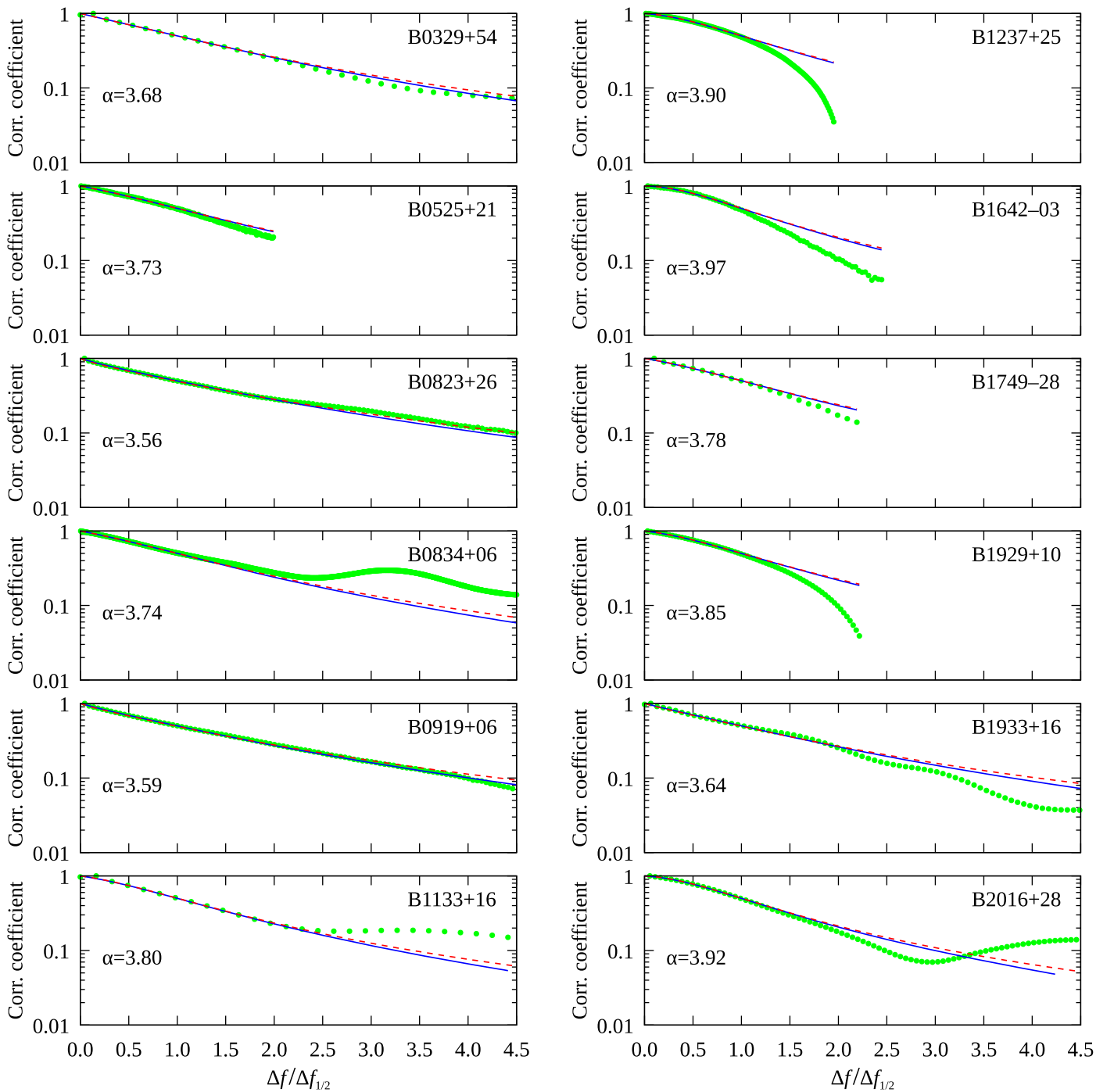


Figure 5. Comparison of the ACF(Δf) functions derived from our observations (green dots) with the best-fit theoretical predictions for the extended-medium model with power-law spectral index α as a fitting parameter (solid blue lines) and for the thin-screen model (dashed red lines) with the same spectral index for comparison. For better comparison all functions were normalized by their HWHM frequency lags, $\Delta f_{1/2}$. Only the inner part of the ACFs down to 45% or up to $\Delta f/\Delta f_{1/2} \sim 1.2$ for which a good fit could be obtained for all pulsars was used for the fit. The parameter, α , which is essentially the same for our ACFs for both models for the fitting range is given for each pulsar. For some pulsars the width of the scintles in terms of $\Delta f_{1/2}$ relative to the receiver bandwidth of 16 MHz was relatively large so that only a shortened version of the functions was plotted.

An alternative approach to search for differences is to analyze the Fourier transform of the ACFs, $\mathcal{FT}[\text{ACF}(\Delta f)]$ (e.g., Armstrong & Rickett 1981; Wolszczan 1983) and the respective thin-screen and extended-medium models as shown in Figure 4. Differences between the models are somewhat more pronounced than in Figure 5. However, also in this case the observed functions $\mathcal{FT}[\text{ACF}(\Delta f)]$ could not conclusively discriminate between either of the models.

3.5. Relation to the Dynamic Visibility Function from Space VLBI Radioastron Observations

The visibility function, $V(\tau, t)$, as a function of delay and time in our space VLBI observations is obtained from the inverse Fourier transform of the cross-spectrum of two different radio telescopes. In our case of observations of dynamic spectra with single telescopes, the cross-spectrum corresponds to the autospectrum at any particular time, t , in a

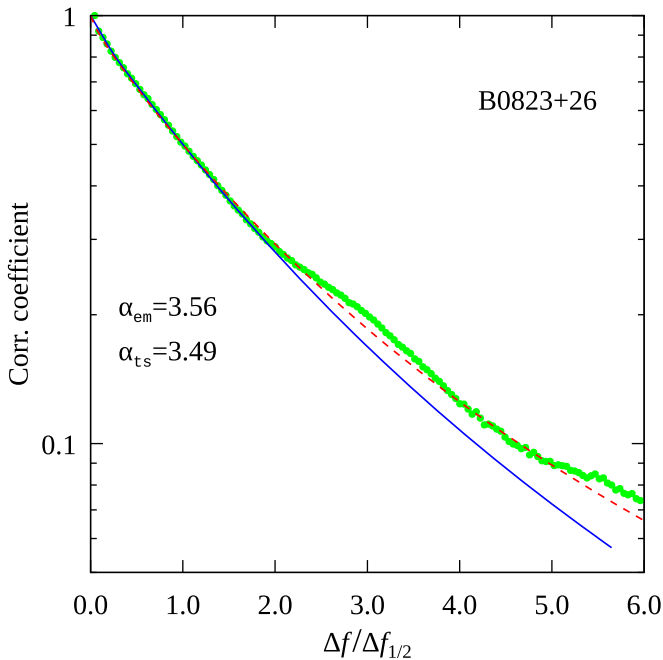


Figure 6. The $ACF(\Delta f)$ function (thick green line) for PSR B0823+26 compared with the extended-medium (solid blue curve) and thin-screen model (dashed red curve) but for frequency lags up to about $6 \times \Delta f / \Delta f_{1/2}$. The extended-medium model is drawn as in Figure 5 with $\alpha_{em} = 3.56$. The thin-screen model is plotted for $\alpha_{ts} = 3.49$ as a test, in an attempt to match the tail of the ACF without excessively changing the best-fit value of $\alpha = 3.56$.

dynamic spectrum, $S(f, t)$. A Gaussian has been used to approximate the frequency section of the ACFs of dynamic spectra (e.g., Cordes 1986). Since for a Gaussian ACF, the underlying function and its Fourier transform are also Gaussians, the autospectrum would also be expected to be a Gaussian. Table 4 lists the function, y , as a Gaussian function, $G(f)$, together with three other functions, $L(f)$, $E(f)$, and $K(f)$, that we consider further in our analysis. In addition we list for each function, y , its Fourier transform, $\mathcal{FT}(y) = \tilde{y}$, and its $ACF(y)$.

Space VLBI with Radioastron revealed for some pulsars that the tail of the delay cross-section of $V(\tau, t)$ retained significant magnitudes at baseline projections where the pulsar scattering disk was completely resolved. The delay cross-section, $ACF(\Delta\tau, \Delta t = 0)$ of $V(\tau, t)$, was found to be well approximated by a Lorentz function (Popov et al. 2020). The Fourier transform of a Lorentz function is a two-sided exponential and therefore the autospectrum from our $S(f, t)$ would also be expected to be a two-sided exponential (second row in Table 4). The ACF of such an exponential, $ACF(E)$, is a function given in the third row in Table 4.

Independent of any prior knowledge from space VLBI observation, an inspection of our observed ACF functions in Figure 3 indicates that several of them have up to $\sim 0.5 \times \Delta f_{1/2}$ a concave profile, with a rounded top where the second derivative is negative. Such a profile is similar to the analytical functions $ACF(G)$, $ACF(L)$, and $ACF(E)$ in Table 4. Some others have in contrast a convex inner profile where the second derivative is positive. This profile is similar to $ACF(K)$.

In Figure 7 we plot as examples the observed ACFs of four pulsars that define the range in curvature for all 12 pulsars and compare them to the four analytical $ACF(y)$ functions. PSR 1642-03 has the most concave inner ACF of all pulsars: it is

between that of the $ACF(G)$ and $ACF(E)$ functions. For the inner part it resembles $ACF(E)$ and for the outer part of the plot it lies between $ACF(E)$ and $ACF(G)$. For PSR 2016+28, the ACF is closest to $ACF(L)$ and $ACF(E)$ for the inner part and lies between the two functions for the outer part. The least ambiguous case is found for PSR 0329+54. The ACF is well matched by $ACF(K)$. PSR B0823+26 has the most convex ACF, even slightly more so than $ACF(K)$. In Table 2 we list the rms values of the observed ACFs to the closest analytical $ACF(y)$ functions and indicate which functions they are. The residuals for all pulsars vary between rms values of 0.0015 for B0329+54 and 0.037 for B1749-28. They are all larger by a factor 2 to 9 than those for the scattering models, however they are also from a fit over a larger lag range and do not have a free parameter for adjustment. In general the ACFs of all 12 pulsars are approximately within the range of the four analytical functions.

Does the ACF of any of these pulsars resemble a Gaussian? We fit a function of the form $f_g(\Delta f) = \exp(-|\Delta f|^\delta / b_f)$ to the ACF of PSR B1642-03, which is one of the two most likely candidates for its ACF to have a Gaussian shape. We obtained for the free exponent and its statistical error $\delta = 1.79 \pm 0.03$, still significantly smaller than $\delta = 2$ for a Gaussian. However, in general it appears that for a few pulsars with a concave shape of the inner ACFs there can be a tendency in the shape of the ACF toward a Gaussian.

Listing the 12 pulsars according to the shape of their ACFs it is clear that the most concave inner ACFs are related to the highest values of α and the most convex to the lowest value. PSR B0823+26 has the most convex ACF, even slightly more so than $ACF(K)$, and the lowest value of α of 3.56. At $\alpha \sim 3.75$ the ACFs transition from concave to convex.

3.6. The Average Frequency Profile of the Scintles

The average frequency profile of the scintles could be obtained analytically by finding the function y in Table 4 if our observed ACFs were exactly represented by $ACF(y)$. However, only very few can be approximately associated with one particular $ACF(y)$, and then only for a limited range of frequency lags. Most are between neighboring analytical functions or are closer to one function in their inner parts and to another function at the tail. Therefore it is best to use the comparison of the observed ACFs with the analytical functions as a guide. The inferences as to the scintle profile can only be approximate.

In Figure 8 we plot the functions, y , which are the underlying functions to $ACF(y)$. The functions G and L are concave up to $\sim \text{HWHM}$ with a bell-shaped profile and the other two functions, E and K , are convex with a profile of a cusp either with a moderate or an extreme peak. In the latter case, the function goes to infinity for $f \rightarrow 0$.

Comparing the $ACF(y)$ with the y functions in Figures 7 and 8 and Table 4, it is clear that the observed ACFs matched best by $ACF(G)$ and $ACF(L)$ functions are associated with bell-shaped scintle profiles. The $ACF(E)$ function is almost identical to $ACF(L)$ for small lags and becomes clearly different for lags $\Delta f > \Delta f_{1/2}$. However, the function y assumes the shape of a cusp. Five of our pulsars have clear similarities to $ACF(E)$ but also to any of the other two functions, G and L . The scintle profile is probably described best as a hybrid between a bell-shaped curve and a cusp.

Table 4
Fourier Transform and Self-convolution of Four Parametric Families of Functions

Name	y	\tilde{y}	ACF(y)
Gauss	$G(\sigma, f) = \frac{\exp(-f^2/(2\sigma^2))}{\sqrt{2\pi}\sigma}$	$\frac{G(1/(2\pi\sigma), t)}{\sqrt{2\pi}\sigma}$	$G(\sqrt{2}\sigma, \Delta f)$
Lorentz	$L(\lambda, f) = \frac{\lambda}{\pi(\lambda^2 + f^2)}$	$\frac{E(1/(2\pi\lambda), t)}{\pi\lambda}$	$L(2\lambda, \Delta f)$
Laplace	$E(\epsilon, f) = \frac{\exp(- f /\epsilon)}{2\epsilon}$	$\frac{L(1/(2\pi\epsilon), t)}{2\epsilon}$	$(\epsilon + \Delta f)E(\epsilon, \Delta f)$
Bessel	$K(\phi, f) = \frac{1}{\pi\phi} K_0\left(\frac{ f }{\phi}\right)$	$\left(\frac{L(1/(2\pi\phi), t)}{2\phi}\right)^{1/2}$	$E(\phi, \Delta f)$

Note. Name of the function, y , definition of y , Fourier transform of y with $\mathcal{FT}(y) = \tilde{y}$. The Fourier transform is defined here as $\tilde{y}(p, t) = \int_{-\infty}^{+\infty} y(p, f) e^{-2\pi ift} df$, with p as a parameter. All the functions considered here are real and normalized so that $\tilde{y}(0) = 1$. Therefore, the ACF is identical with self-convolution and $\widetilde{\text{ACF}} = \tilde{y}^2$. Because of the normalization chosen, the functions may be identified with probability densities of random variables. The functions named ‘‘Lorentz,’’ ‘‘Gauss,’’ and ‘‘Laplace’’ are related to the well-known statistical distributions whose mathematical properties are described by Feller (1971). For the last row, we used the term ‘‘Bessel’’ for the function since $K_0(z)$ is the modified Bessel function of the second kind of order 0 and argument z which rises logarithmically to infinity at $f \rightarrow 0$. The scale parameters σ and ϕ are equal to rms deviations of the corresponding distributions, and the parameters λ and ϵ are half-widths of the Lorentz and Laplace distributions at the level 1/2 and 1/e, respectively.

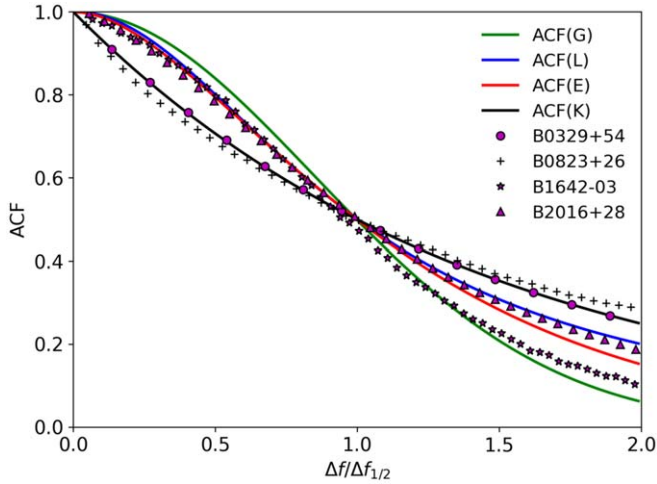


Figure 7. The four ACF(y) functions listed in Table 4 and plotted as a function of frequency lag Δf . The functions are normalized in amplitude and with respect to their HWHM, $\Delta f_{1/2}$, for easy comparison. All functions are two-sided; only one side is plotted. In addition, observed ACFs are plotted for four pulsars to display the range of ACF variations for comparison.

For one pulsar, B1929+10, the ACF is best described only by ACF(E). None of the observed ACFs is best described only by the bell-shaped functions, G and L . For three pulsars, B0525+21, B1133+16, and B1749+28, there is a transition from concave to convex ACF shapes. Their ACFs are hybrids with ACF(K) as one element. For five other pulsars their ACFs are clearly convex and best described by only ACF(K). The scintle profile is less ambiguous. Although the function, K , goes to infinity for $f \rightarrow 0$, because of deviations of the observed ACFs from ACF(K), the scintle profile would probably be best described as a pronounced cusp with a sharp peak.

What is the relation of the wavenumber power-law spectral index to the scintle profile? It appears that for pulsars with high α values, that is, steep wavenumber spectra, the scintle could have a profile intermediate between a cusp and a Gaussian or Lorentzian because of a tendency of the shape of their ACFs toward these functions. Below the transition from a concave shape of the inner ACFs to a convex shape at $\alpha \simeq 3.75$ the cusp becomes more clearly defined with a sharp peak and its sides

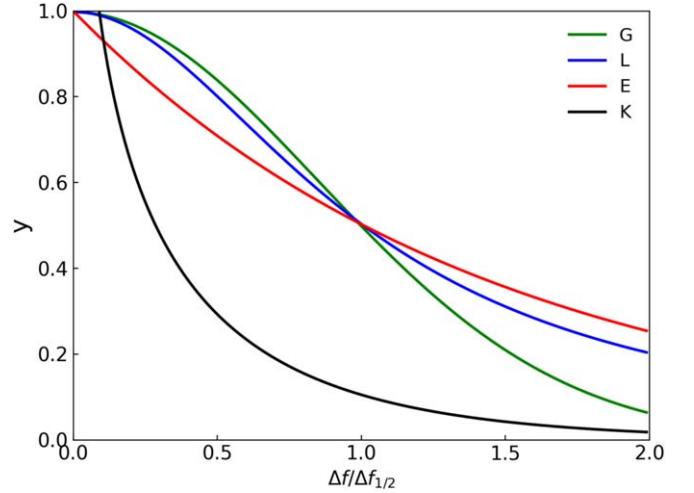


Figure 8. The four functions, y , in Table 4 plotted as a function of frequency, f . Three functions are normalized in amplitude and width to facilitate comparison. The fourth function, K , is plotted with the respective normalization parameter corresponding to the function, E . It goes to infinity at $f \rightarrow 0$. As in Figure 7, all functions are two-sided; only one side is plotted.

decrease even faster than exponentially in the case of pulsars with the flattest wavenumber spectra.

4. Discussion

The electron density variations in terms of the wavenumber power-law spectral index, α , can be estimated by several methods by, for example, analyzing the shapes of ACFs of dynamic spectra in frequency and time, the frequency dependence of the decorrelation bandwidth, $\Delta f_{1/2}$, the scattering time, τ_{sc} , and the scattering angle, θ_{sc} . We estimated the index, α , for 12 pulsars by analyzing the frequency section of the time-averaged ACF of dynamic spectra and comparing it to extended-medium and thin-screen scattering models. This is the largest sample we are aware of that has been used for such analysis and has given us important insight into the characteristics of the turbulent interstellar plasma and the associated frequency profile of the scintles.

The inner part of the ACFs of all 12 pulsars down to at least 45% of the maximum or $1.2 \times \Delta f_{1/2}$ is for most pulsars well fit

by the predictions of the extended-medium and thin-screen scattering theories. The power-law spectral indices range from $\alpha = 3.56$ to 3.97 with errors ≤ 0.05 and a mean with standard deviation of 3.76 ± 0.13 , which is close to the index of 3.67 for the Kolmogorov spectrum. The largest deviations from either of the models were found for PSR B1642-03 with an error for α of 0.05 .

All pulsars show deviations of their ACFs from either of the models at frequency lags starting at ~ 1.2 to $3 \times \Delta f_{1/2}$. These deviations are larger than any found for the inner part of the ACFs. For some of them the ACFs turn to a level above the models, which could possibly be due to technical reasons. However, for most of them the ACFs turn to a level clearly below the models, which likely has physical reasons. A more compact ACF is equivalent to a broader $\mathcal{FT}(\text{ACF})$ (compare Figures 4 and 6). Longer delays correspond to more compact inhomogeneities, which may indicate deficiencies in either of the two scattering models.

The most direct comparison of our measurements of α are those obtained from $\mathcal{FT}[\text{ACF}(\Delta f)]$. While the estimates of Armstrong & Rickett (1981) have rather large allowed ranges, the estimates of Wolszczan (1983; no errors given), are equal within our errors of 0.1 . Although only three pulsars could be compared, this result is remarkable, since the observations were made some 30 years apart and therefore give hints as to the stability of the power-law spectrum for the direction of these pulsars.

Of particular interest is a comparison of an estimate of α by Popov & Smirnova (2021), who used for 10 of our pulsars the same dynamic spectra but focused on the time section of the frequency-averaged ACFs and analyzed the structure function. While for five pulsars their values are only somewhat larger or smaller within a difference of ≤ 0.10 , for the other pulsars their values are all smaller by as much as 0.51 in the case of B1237+25. Such large discrepancies are remarkable given that the estimates were obtained on the basis of the same spectra but separately for their frequency and their time characteristics.

The estimates of α from the frequency dependence of $\Delta f_{1/2}$ as given in our example in Table 3 were largely consistent with our values, albeit within the authors' (Cordes et al. 1985) larger errors.

Independent information on α comes from measurements of the exponential broadening of pulses through multiple path propagation in the ionized ISM. The parameterization is generally given by the broadening timescale or scattering time, τ_{sc} . This parameter in turn is related to α . For a power-law wavenumber spectrum, $\tau_{\text{sc}} \propto f^{-\beta}$, and for $\alpha < 4$, $\beta = 2\alpha/(\alpha - 2)$. That requires $\beta > 4$. Löhmer et al. (2004) found for seven pulsars $3.3 \leq \alpha \leq 4.0$ and for PSR B1933+16, in our list, $\beta = 3.4 \pm 0.2$, too small for $\alpha < 4$. Bhat et al. (2004) found for eight out of 15 pulsars $3.1 \pm 0.7 \leq \alpha \leq 4 \pm 1$ but for the others also values of β too small for $\alpha < 4$. An even larger portion of pulsars outside the α range was found by Geyer et al. (2017), with $1.5 \leq \beta \leq 4.0$ for 13 pulsars and only two of them with $\alpha < 4$ within the errors. The largest sample of pulsars with multifrequency observations was obtained by Lewandowski et al. (2015). From 48 pulsars only 16 were given with values of α within their errors $\lesssim 4$, including the only one from our list, PSR B1749-28, with $\alpha = 4.24 \pm 0.18$, different from our value of 3.78 ± 0.02 by 3 times their larger uncertainty. All the others, including PSRs B1642-03 and B1933+16 from our list, had correspondingly smaller values of β , with an average of 3.89 .

The consistent result from pulse-broadening observations is that a large fraction of pulsars have β values too small to be consistent with $\alpha < 4$. Several effects could be considered that would lead to an increase or changes of β . There is an indication that pulsars with a dispersion measure < 500 pc cm^{-3} have with $\beta = 3.95$ a larger average than those with a dispersion measure > 500 pc cm^{-3} with $\beta = 3.49$ (Lewandowski et al. 2015). All of our pulsars have in comparison very small dispersion measures (see Table 2). Geyer et al. (2017) find that their small values of β may be indications of anisotropic scattering since that assumption would lead to an increase of the values. Anisotropic scattering mechanisms have also been considered by Stinebring et al. (2001) and Tuntsov et al. (2013). Other effects discussed include finite or truncated scattering screen (Cordes & Lazio 2001) and internal cutoff scale effects (Rickett et al. 2009). Also, analysis of the structure function of several pulsars, based on multifrequency observations, shows that the spectrum of interstellar plasma in the direction of some pulsars follows a piecewise power law (Shishov et al. 2003; Smirnova et al. 2006). Our measurements of 12 pulsars with a different analysis scheme adds to the discussion of the wavenumber spectrum and the electron density variations of the plasma turbulence of the ISM. In general it appears that more complex theoretical models are needed to describe the observed data, or possibly that there are deviations from the wavenumber power-law spectrum.

In our search for the average frequency profile of the scintles in terms of analytical functions independent of scattering models we were guided by our earlier results from VLBI observations of pulsars, where we found that the delay section of the visibility function of some pulsars could be well fit by Lorentzians. For half of our pulsars we indeed found that the ACFs could be best fit by the corresponding $\text{ACF}(E)$ function or by a hybrid of functions with $\text{ACF}(E)$ being part of it. However, for five others the more sharply pointed two-sided exponential, $\text{ACF}(K)$, was warranted in addition to three more where that function was part of a hybrid. It is interesting to note that while the set of power-law spectral indices from $\alpha = 3.97$ to 3.56 appears to be a uniform distribution, the functions describing the ACFs and the shape of the scintles are at least formally quite different. For the steep spectra with $\alpha \gtrsim 3.75$ the inner part of the ACFs become increasingly concave, while for the flatter spectra with $\alpha \lesssim 3.75$ they become convex. In other words, the value of α determines the average frequency profile of the scintles. Steep wavenumber spectra with $\alpha < 4$ correspond to scintles with a somewhat rounded cusp. With smaller α values the peak of the cusp becomes more pronounced. For $\alpha \lesssim 3.75$ and further flattening, the cusp and its peak sharpen further and decay faster than an exponential, approaching at least nominally the modified Bessel function of the second kind of order zero.

Is there any correlation between the shape of the scintles and any of the pulsar characteristics listed in Table 1, such as the dispersion measure, the distance to the pulsar, and the galactic coordinates? We searched for such a correlation but no correlation is apparent.

5. Conclusions

1. We analyzed the dynamic spectra of nine pulsars at a center frequency of 324 MHz and three pulsars at

1676 MHz and computed the frequency sections of the two-dimensional ACFs.

2. For each pulsar the inner part of the function down to at least 45% of the maximum is well fit by the prediction of a thin-screen or extended-medium scattering model. The power-law wavenumber spectral indices of the interstellar plasma turbulence, α , are all within a range of 3.56 and 3.97 with uncertainties ≤ 0.05 .
3. The mean of the spectral indices with standard deviation is $\langle \alpha \rangle = 3.76 \pm 0.13$, which is close to the Kolmogorov index of 3.67.
4. The Fourier transforms of the model functions fit to those of the ACFs for the full width gives similar values for α , although with larger uncertainties.
5. Beyond the inner part of the function, clear misfits can be seen for all of our pulsars that are larger than any possible deviations seen in the inner part of the ACFs, indicating scattering characteristics more complex than described in the models, or indicating that there are deviations from the power law of the interstellar plasma turbulence.
6. Comparison of extended-medium and thin-screen models with observed ACFs and the respective $\mathcal{FT}(\text{ACF})$ s gives no clear evidence that either of the models is preferred.
7. The observed ACFs have a concave inner part down to about half of the maximum for high α values that becomes less concave with flattening spectra and turns convex for $\alpha \lesssim 3.75$.
8. For six pulsars with $3.75 \lesssim \alpha < 4.0$, the function $\text{ACF}(E)$ alone or as a member of a hybrid fits the observed ACFs moderately well down to 20% of the maximum. This function is expected for pulsars for which the Lorentzian provides a fairly good fit to the visibility function from VLBI.
9. For the pulsars with $3.56 \leq \alpha \lesssim 3.75$ a function like the two-sided exponential, $\text{ACF}(K)$, is more warranted for the fit to the ACFs.
10. A Gaussian was not an appropriate fit for any of the ACFs of the 12 pulsars. The pulsars which came closest are B1237+25 and B1642-03, with ACFs described best by a hybrid between $\text{ACF}(G)$ and $\text{ACF}(E)$.
11. From the functional fit to the observed ACFs we found that the average frequency profile of a scintle is for steep wavenumber spectra characterized by a hybrid between a cusp and a function like a Gaussian or Lorentzian. With increasing flattening of the spectrum with $\alpha \lesssim 3.75$, the cusp and its peak becomes more pronounced and decays faster than an exponential.

We thank an unknown referee for their valuable comments and suggestions. The Radioastron project is led by the Astro Space Center of the Lebedev Physical Institute of the Russian Academy of Sciences and the Lavochkin Scientific and

Production Association under a contract with the Russian Federal Space Agency, in collaboration with partner organizations in Russia and other countries. This paper was supported in part by the Russian Academy of Science Program KP19-270, “The study of the Universe origin and evolution using the methods of earth-based observations and space research.” N.B. was supported by the National Sciences and Engineering Research Council of Canada.

Facilities: Arecibo, Green Bank (GBT), Parkes, Westerbork.
Software: CFITSIO.

ORCID iDs

M. S. Burgin  <https://orcid.org/0000-0002-0579-2938>

References

- Armstrong, J. W., & Rickett, B. J. 1981, *MNRAS*, 194, 623
 Backer, D. C. 1975, *A&A*, 43, 395
 Bhat, N. D. R., Cordes, J. M., Camilo, F., Nice, D. J., & Lorimer, D. R. 2004, *ApJ*, 605, 759
 Chashei, I. V., & Shishov, V. I. 1976, *SvA*, 20, 13
 Cordes, J. M. 1986, *ApJ*, 311, 183
 Cordes, J. M., & Lazio, T. J. W. 2001, *ApJ*, 549, 997
 Cordes, J. M., Weisberg, J. M., & Boriakoff, V. 1985, *ApJ*, 288, 221
 Fadeev, E. N., Andrianov, A. S., Burgin, M. S., et al. 2018, *MNRAS*, 480, 4199
 Feller, W. 1971, *An Introduction to Probability Theory and its Applications*, Vol. 2 (2nd ed.; New York: Wiley)
 Geyer, M., Karastergiou, A., Kondratiev, V. I., et al. 2017, *MNRAS*, 470, 2659
 Goodman, J., Romani, R., Blandford, R., & Narayan, R. 1987, *MNRAS*, 229, 73
 Gwinn, C. R., Popov, M. V., Bartel, N., et al. 2016, *ApJ*, 822, 96
 Kardashev, N. S., Alakoz, A. V., Andrianov, A. S., et al. 2017, *SoSyR*, 51, 535
 Lee, L. C., & Jokipii, J. R. 1975a, *ApJ*, 196, 695
 Lee, L. C., & Jokipii, J. R. 1975b, *ApJ*, 201, 532
 Lee, L. C., & Jokipii, J. R. 1975c, *ApJ*, 202, 439
 Lerche, I. 1979, *MNRAS*, 189, 137
 Lewandowski, W., Kowalińska, M., & Kijak, J. 2015, *MNRAS*, 449, 1570
 Löhmer, O., Mitra, D., Gupta, Y., Kramer, M., & Ahuja, A. 2004, *A&A*, 425, 569
 Lovelace, R. V. E. 1970, PhD thesis, Cornell Univ.
 Narayan, R. 1992, *RSPTA*, 341, 151
 Popov, M. V., Andrianov, A. S., Bartel, N., et al. 2016, *ARep*, 60, 792
 Popov, M. V., Bartel, N., Burgin, M. S., Smirnova, T. V., & Soglasnov, V. A. 2021, *MNRAS*, 506, 4101
 Popov, M. V., Bartel, N., Burgin, M. S., et al. 2020, *ApJ*, 888, 57
 Popov, M. V., Bartel, N., Gwinn, C. R., et al. 2017, *MNRAS*, 465, 978
 Popov, M. V., & Smirnova, T. V. 2021, *ARep*, 65, 1129
 Rickett, B., Johnston, S., Tomlinson, T., & Reynolds, J. 2009, *MNRAS*, 395, 1391
 Rickett, B. J. 1977, *ARA&A*, 15, 479
 Romani, R. W., Narayan, R., & Blandford, R. 1986, *MNRAS*, 220, 19
 Shishov, V. I., Smirnova, T. V., Sieber, W., et al. 2003, *A&A*, 404, 557
 Smirnova, T. V., Shishov, V. I., Sieber, W., et al. 2006, *A&A*, 455, 195
 Stinebring, D. R., McLaughlin, M. A., Cordes, J. M., et al. 2001, *ApJL*, 549, L97
 Tuntsov, A. V., Bignall, H. E., & Walker, M. A. 2013, *MNRAS*, 429, 2562
 Wolszczan, A. 1983, *MNRAS*, 204, 591